*Article*

# Date Palm Seed Extract for Mild Steel Corrosion Prevention in HCl Medium

Naba Jasim Mohammed [1,*] , Norinsan Kamil Othman [1,*] , Ahmed Jamal Abdullah Al-Gburi [2] and Rahimi M. Yusop [3]

1 Materials Science Program, Department of Applied Physics, Faculty of Science and Technology, University Kebangsaan Malaysia, Bangi 43600, Selangor, Malaysia

2 Faculty of Electronics and Computer Engineering, Universiti Teknikal Malaysia Melaka, Hang Tuah Jaya, Durian Tunggal 76100, Melaka, Malaysia

3 Faculty of Science and Technology, School of Chemical Sciences and Food Technology, University Kepangsaan Malaysia, Bangi 43600, Selangor, Malaysia

* Correspondence: naba_jasem@yahoo.com (N.J.M.); insan@ukm.edu.my (N.K.O.)

**Abstract:** The inhibition effects of the date palm seed extract corrosion of mild steel in 0.5 M HCl at different concentrations are investigated by potentiodynamic polarisation (PDP), electrochemical impedance spectroscopy (EIS) and weight loss tests. Additionally, this study provides a fundamental understanding of aromatic adsorption on iron (Fe) surfaces. Furthermore, the surface morphology and the extracts are performed using scanning electron microscopy (SEM) and Fourier transform infrared spectroscopy (FTIR). The maximum inhibition efficiency of 95, 96, and 91% were realised at 1400 mg/L for PDP, EIS, and weight loss, respectively. The inhibitive action of the DPS extract against mild steel corrosion in an acid solution has been supported by SEM analysis. The FTIR showed that the extract contained hydroxyl ($-$OH) and methoxyl ($-$OCH$_3$) functional groups. The DFT depicted the adsorption sites at the oxygen (O) and carbon (C) atoms as deduced from the Fukui functions, Mulliken atomic charge, and the highest occupied molecular orbital-lowest occupied molecular orbital (HOMO-LUMO) analysis. The DPS preferred to form chemical bonds by donating electrons to the Fe surface. The coordinate bonds between the O and C atoms and the metal surface resulted in a high inhibition efficiency value. In conclusion, date palm seed extract is an effective inhibitor to protect mild steel from corrosion in an acidic medium.

**Keywords:** date palm seed; corrosion prevention; electrochemical studies; mild steel; HCl

## 1. Introduction

Hydrochloric acid (HCl) solution including other acids is generally used to remove rust and the scale of industrial methods, while HCl is commonly used in the processes of metal pickling. Inhibitors are explicitly used in acid solutions to prevent corrosion, metal dissolution, and acid consumption [1]. However, HCl or any acid implementation issue in this process lies in the use of acid treatment, which accelerates the corrosion rate in gas and oil fields [2]. Importantly, acid is essential in the inhibition of the corrosion rate for gas and oil wells in the acid treatments [3]. Preventing corrosion is not free, but it is less costly than fixing or replacing damaged systems when it is too late. Without preventative steps, facilities can become damaged. Corrosion of steel is a severe problem as it negatively affects desirable steel properties, which lose its strength and become unfit for further use. This leads to the damage and wastage of tons of steel. Synthetic corrosion inhibitors have been used to control corrosion alloys, but they harm humans, aquatic life, and the environment. Some chemicals also cause irreversible harm, such as mutations in human genes, carcinogenesis, and reproductive or foetal toxicity. As a result, corrosion inhibitors derived from natural extracts to protect metals and alloys from corrosion are critical to reducing the risks to humans and the environment.

Green corrosion inhibitors are bioactive natural materials without any hazardous chemicals. They can be used without causing harm to the transportation system. Adding small amounts of corrosion inhibitors to the environment will reduce, slow down, or prevent metal corrosion. One of the finest methods for controlling the corrosion of metals and alloys is the use of inhibitors. Green corrosion inhibitors are being sought after because they are biodegradable, in contrast to inorganic corrosion inhibitors which damage the environment [4].

Corrosion inhibitors are commonly used in acidic mediums. Furthermore, although the main organic compound inhibitors consist of heteroatoms, including O, N and S, which could be absorbed into the metal surface, the use of corrosion inhibitors continues today. Plant extracts are rich in natural sources, leading to their excellent function as corrosion inhibitors. These extracts are also environment-friendly, renewable, inexpensive, and readily available, so the seed and plant extracts could be applied as green corrosion inhibitors. Numerous reports have recently been published on the use of various plants as green corrosion inhibitors for acidic mediums with high inhibition efficiency (IE%). To illustrate, Punica Plant extract displayed an 84.5% inhibition efficiency at 300 mg/L concentration level [5], Psidium Guajava Leaf extract showed an 82% inhibition efficiency at 1200 mg/L [6], Rice Husk extract exhibited an inhibition efficiency of 86% [7], Ginkgo leaves extract displayed an inhibition efficiency of 78% at 1200 mg/L [8], Capsicum frutescens Biomass extract showed an inhibition efficiency of 85.5% at 1000 mg/L [9]. Radish seeds aqueous extract displayed a 54.2% inhibition efficiency at 10% *v/v* [10]. The Akebia trifoliate koiaz peels extract in in HCl solutions, and the maximum IE% was 89.2 at 800 mg/L [11].

Meanwhile, the extract of Murraya koenigii leaves displayed a 97.5% inhibition efficiency at 600 mg/L [12], Chenopodium Ambrosioides extract in sulfuric acidic solution exhibited an 89% inhibition efficiency at 4 g/L [13], and Butea monosperma extract in 0.5 M $H_2SO_4$ displayed a 98% inhibition efficiency at 500 mg/L concentration level [14]. On the other hand, pendula leave extract in 1 M HCl exhibited a 93% inhibition efficiency at 0.4 g/L [15]. In a study conducted by the authors of [16], the Rollinia occidentalis extract used for carbon steel in an HCl solution displayed a 79.7% inhibition efficiency. Notably, several reports were made in studies regarding the function of date palm waste extract as a corrosion inhibitor. These could be seen from [17] on Palm leaf and Palm fibre for the same functions and an investigation by [18,19], where the juice of date palm was used in 3.5% of NaCl solution for aluminium alloy. However, few reports were made regarding the application of the waste of date palm extract as a corrosion inhibitor in 0.5 M HCl for mild steel.

Date palm (*Phoenix dactylifera*) is a natural resource that produces healthy fruit, possesses good medicinal value, and functions as a staple diet in most parts of the Middle East and North Africa. The date palm fruits are edible, but the seeds are inedible and not in use. However, the applied research uses agricultural waste to produce green corrosion inhibitors and replace synthetic corrosion inhibitors, which are dangerous, hurtful, and toxic to humans and the environment. The date palm seed has been chosen because it is rich in fatty acids (lauric, myristic, oleic, phthalic, caprylic, and palmitic acids) as indicated in our research group [20,21], which contain heteroatoms compounds in their molecular structure and provide more active centres in their structures and will provide easy adsorption on the metal surface. Thus, active substances such as corrosion inhibitors are a subject of great practical significance. It was also proven from this study that the seeds are valuable as green corrosion inhibitors. Following that, an evaluation was conducted on the corrosion inhibition efficiency of the DPS for mild steel in 0.5 M HCl solution using potentiodynamic polarisation and electrochemical impedance spectroscopy (EIS) measurements at 25 °C. Using experimental methods to examine the relationship between a corrosion inhibitor and its inhibition efficiency (IE%) is insufficient, costly, and time-consuming. It is more economical and faster to use computational techniques such as quantum chemical simulations and density functional theory (DFT) as predictive tools. The novelty of this work is as follows: (1) the use of agricultural waste, which is date palm seeds, as green

corrosion inhibitors to replace synthetic and expensive corrosion inhibitors; (2) this inhibitor inhibited mild steel corrosion in 0.5 M HCl with a 96% inhibition efficiency. Hence, this work can reduce the costs related to acidic corrosion and support the acidising treatment, increasing the wells' productivity and maximising the recovery of oil/gas. Therefore, this inhibitor is highly required in the oil and gas industry. (3) This study applied quantum chemical calculations to screen adsorption sites on inhibitors and determine the atoms' local reactivity in corrosion inhibitors.

## 2. Materials and Methods

### 2.1. Date Palm Seeds (DPS) Extraction

In this stage, the date palm seed was extracted as follows. The date palm seed was washed and sun-dried for a few days before being dried in an oven at 40–50 °C for 20–30 min. The dried date seed was then mechanically processed into a powder. On a hot plate, 10 g of seed powder was diluted in 1 L of 0.5 M HCl media at 50 °C for 15 h while being continuously magnetically stirred [22]. Throughout the extraction, the solution was monitored for temperature uniformity and solubility. The solution was then filtered to remove any remaining solid particles, and then the HCl solvent was removed from the extraction solution using a rotary evaporator below 50 °C, as seen in Figure 1. Finally, the water content from the extraction was dried using the oven on the petri dish. The drying methods were carried out at 60 °C for about 3 h.
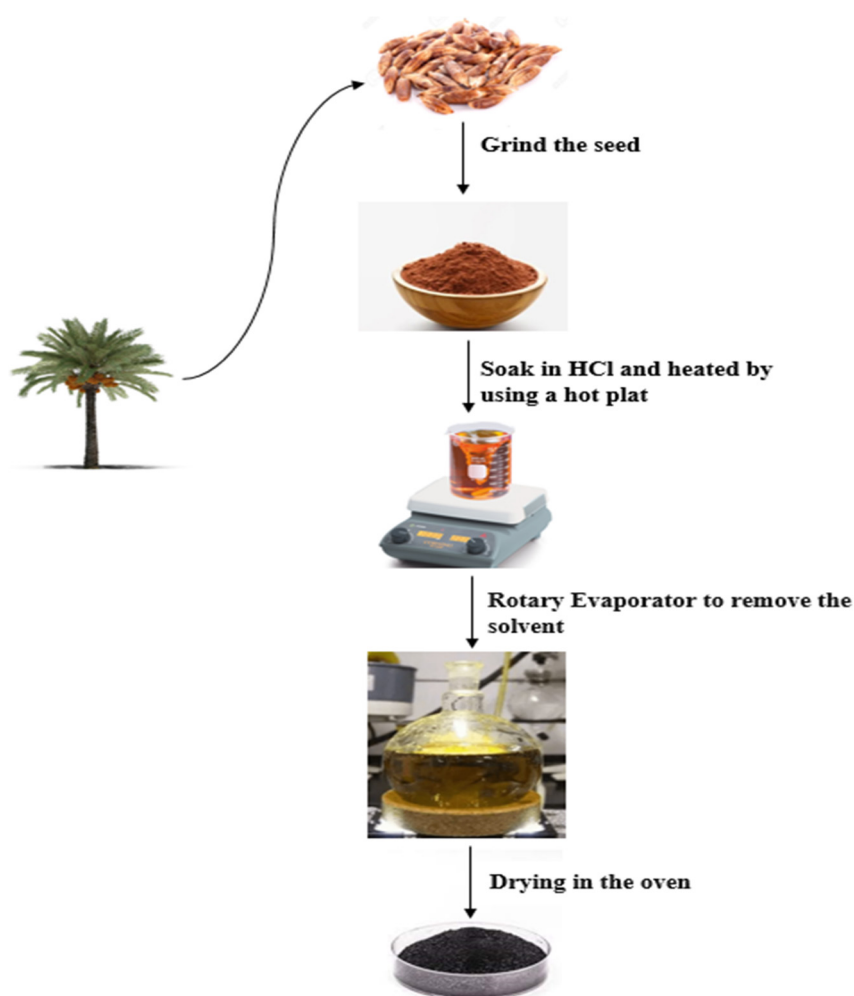


**Figure 1.** Flow chart of the extraction process.

## 2.2. Preparation of Mild Steel

Experiments were performed using mild steel, which consisted of a wt% composition of C 0.08%, P 0.014%, S 0.018%, Si 0.17, Mn 0.35, and Fe balance. ASTM standard of G1-03 was used to clean up the mild steel. Furthermore, grinding–polishing Machine-Top-Tech-P2554-mecapol was used to rub the samples against Silicon Carbide papers, with grades ranging from 400 to 1200. To obtain the mirror brightness, cotton with buffing soap was used, followed by a washing process through distilled water and a drying process using a hairdryer [23].

## 2.3. Electrochemical Studies

The electrochemical test was performed to assess corrosion efficiency via three techniques: the open circuit potential (OCP), then potentiodynamic polarisation (PDP), and electrochemical impedance spectroscopy (EIS). This test was performed by using Gamry potentiostat-ZAR Reference-3000, which was ensured with a calibration procedure using an appropriate dummy cell and directed to the Gamry software (see Figure 2). The potentiostat was connected to a three-electrode cell. Graphite was applied as a counter electrode, while a saturated calomel electrode (SCE) was employed as a reference electrode. The last electrode was mild steel, acting as a working electrode, where the specimens were placed in a non-conductive epoxy resin. These samples were smoothed using the tool the size of up to 1200 grit to prepare for the electrochemical test. The mild steel was positioned around the SCE without connecting the electrodes.
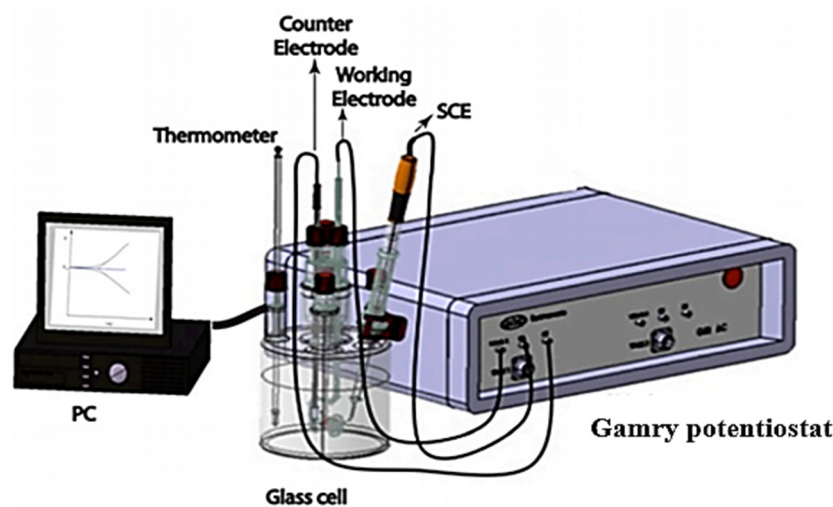


**Figure 2.** Electrochemical setup cell.

### 2.3.1. Open Circuit Potential (OCP)

Two electrodes were immersed in an electrolyte in the electrochemical cell. When the electrodes are electrically connected, the difference in potential between the two electrodes causes a flow of electricity as electrons shift from the lower-potential metal to the higher-potential metal. The material with the lower potential becomes the anode, while the material with the higher potential becomes the cathode.

Open circuit potential (OCP) aims to determine the potential originating over the working electrode without using any external current or potential. OCP is also referred to as "free corrosion potential or mixed corrosion potential". Simply measuring OCP yields minimal information, but EIS and PDP depend on OCP stability; if OCP dramatically changes during EIS and PDP measurements, their usefulness is called into doubt. Therefore, it is imperative to attain a stable OCP value before performing potentiodynamic polarisation and EIS studies.

### 2.3.2. Potentiodynamic Polarisation (PDP)

Potentiodynamic polarisation analyses were carried out to study the anodic and cathode electrochemical reaction with DPS inhibitors in the corrosion medium. These measurements provide information on changes in corrosion ability, corrosion current density ($i_{corr}$), anodic slope ($\beta_a$) and cathodic slope ($\beta_c$). Potentiodynamic polarisation curves were performed by replacing the electrode potential from ($\pm 250$ mV) opposing the open circuit potential ($E_{corr}$) at a scan rate of $0.167$ mVs$^{-1}$. The open-circuit capacity was run for 20 min in each experiment. The 20 min were taken to stabilise the electron flow between the electrode and the inhibitor solution in the circuit. This created a stable state and minimised charge disruption during testing. Polarisation measurements continue to be performed automatically once the open circuit capacity is completed. Once it is completed, the Tafel plot appears on the computer screen, accompanied by analytical information from the Tafel plot. Based on information from polarisation plot analysis, the values of corrosion efficiency (IE%) were calculated using the following Equation [23]:

$$IE\% = 1 - \left( \frac{i_{corr}}{i_{corr}^o} \right) \times 100\% \qquad (1)$$

### 2.3.3. Electrochemical Impedance Spectroscopy (EIS) Technique

The impedance measurement was performed to evaluate the effects of steel corrosion inhibition by DPS taking into account the corrosion resistance that occurs on the steel interface and the solution of the inhibitor. Through this test, charge transfer information and solution resistance were obtained. The frequency zone range starts from 10 KHz to 0.01 Hz, with 17 points per hertz decade and an ac voltage amplitude of $\pm 10$ mV. Moreover, Gamry software automatically controlled the measurements obtained on the rest potentials at 25 °C. The Nyquist and the Bode plots were obtained from measurement. The IE% can be calculated using the following Equation:

$$IE\% = \left( \frac{R_{ct} - R_{ct}^\circ}{R_{ct}} \right) \times 100\%, \qquad (2)$$

where $R_{ct}$ and $R_{ct}^\circ$ are the charges transfer resistance in the presence and absence of DPS inhibitor concentrations.

### 2.4. Weight Loss Test

Different concentrations (800, 900, 1200, 1400, 2000 mg/L) were prepared and used as test solutions to identify the optimum concentration of corrosion inhibitor. The mild steel specimens were weighed before and after immersion in the test solution. The samples were considered by using a digital balance and hung in a 120 mL flask containing 800, 900, 1200, 1400, and 2000 mg/L of corrosion inhibitor in 0.5 M HCl solution at room temperature. After the duration of immersion, the samples were removed from the test media, washed for 10 min with 500 mL HCl + 3.5 g hexamethylene tetraamine + distilled water to obtain 1000 mL, reweighed, and subsequently returned into the desiccator. The difference in weight of the steel samples has been recorded as weight loss [24]:

$$\Delta W = W_i - W_f, \qquad (3)$$

where $\Delta W$ is the difference between the initial ($W_i$) and final ($W_f$) weight of mild steel (g). In the meantime, the corrosion rate was calculated using Equation (4) [25]:

$$C_r \left( \text{mmy}^{-1} \right) = \frac{87600 \times \Delta W}{\rho TA}. \qquad (4)$$

where $\rho$ and A are the density and surface area of mild steel, respectively. The immersion time per hour (h) is denoted as T, and 87,600 is a constant for $C_r$ determination. The IE% was determined using the Equation below:

$$IE\% = \left( \frac{C_{r_{blank}} - C_{r_{inh}}}{C_{r_{blank}}} \right) \times 100, \tag{5}$$

where $C_{r_{blank}}$ and $C_{r_{inh}}$ are the corrosion rates without and with DPS inhibitor concentrations, respectively. The degree of surface coverage ($\theta$) is determined by applying Equation (6):

$$\theta = \left( \frac{C_{r_{blank}} - C_{r_{inh}}}{C_{r_{blank}}} \right). \tag{6}$$

The degree of surface coverage is essential to determine out the coverage ability of each concentration to protect mild steel from corrosion.

*2.5. Fourier Transform Infrared Spectroscopy (FTIR) Technique*

FTIR spectrum was utilised to determine the functional groups in the date palm seed compound. The organic material analysis technique through FTIR is a simple, accurate technique (with high sensitivity and selectivity), fast, and requires only a small sample to analyse. Through this method, the spectra are obtained to provide the signal peak values of each wavenumber range that characterise the type of group functioning in a compound. Therefore, the initial characterisation of the molecular structure of the studied compounds can be identified. Approximately 1 mg of date seed extract powder was placed on the sample stage, and the stage was closed for analysis. During the examination, samples emitted with infrared radiation absorb light and reflect the identity of the components of a group operating on a particular wave. In this study, the wavelength for the spectral spectra was set in the range of 600–4000 cm$^{-1}$. This method is similar to the scattering spectroscopy technique in which data are generated in individual components. Thus, each wave number is the identity of a specific functional group.

*2.6. Computational of Density Function Theory (DFT)*

In order to study the molecular mechanism of corrosion inhibitor, a simulation was carried out. DFT also provided researchers with a better understanding of adsorption and the electric effects that go along with it. DFT is the most outstanding alternative for examining these issues because of the significant changes the corrosion inhibitor might have on the mild steel surface.

2.6.1. Quantum Chemical Calculation

The geometrical optimisation of the inhibitor molecules was carried out within the DFT framework using the DMol3 software and the generalised gradient approximation of the Perdew–Burke–Ernzerhof (GGA-PBE) functional. The computations produced quantum chemical characteristics such as the energy of the lowest unoccupied molecular orbital ($E_{LUMO}$) and the energy of the highest occupied molecular orbital ($E_{HOMO}$). In addition, other quantum parameters such as the energy gap ($\Delta E$), ionisation potential (IP), electron affinity (EA), electronegativity ($\chi$), global hardness ($\eta$) and global softness ($\sigma$) were determined using the formulas below [26]:

$$\Delta E = E_{LUMO} - E_{HOMO}, \tag{7}$$

$$IP = -E_{HOMO}, \tag{8}$$

$$EA = -E_{LUMO}, \tag{9}$$

$$\chi = (IP + EA)/2, \tag{10}$$

$$\eta = \frac{IP - EA}{2},\tag{11}$$

$$\sigma = 1/\eta.\tag{12}$$

The fraction of electrons transferred from the inhibitor to the surface of Fe (110), $\Delta N$, was calculated using Equation (13):

$$\Delta N = (\phi - \chi_{inh})/[2(\eta_{inh})],\tag{13}$$

where $\phi$ equals 4.82, which signifies the work function of the Fe (110) surface [27].

### 2.6.2. Adsorption Sites

Mulliken atomic charges and Fukui functions were computed using the geometry optimised structure. Mulliken population analysis was used to analyse the electrophilic and nucleophilic functions of Fukui. Mulliken atomic charges and Fukui functions were utilised to screen adsorption locations on inhibitors. Fukui functions determined the local reactivity of the atoms in the corrosion inhibitor. The values acquired from Fukui functions can be used to identify atoms in a molecule with higher reactivity to receive and lose electrons.

## 3. Results

### 3.1. Open Circuit Potential Analysis (OCP)

The OCP can be defined as the working electrode's potential concerning the reference electrode without applied current. Before performing the PDP and EIS studies, it is essential to keep the OCP stable. The results of OCP measurements on mild steel corrosion in 0.5 M HCl with and without different concentrations of DPS are depicted in Figure 3. Straight OCP curves suggest the dissolution of the mild steel oxide layer and the adsorption of the DPS corrosion inhibitor that interfaces metal and electrolyte.
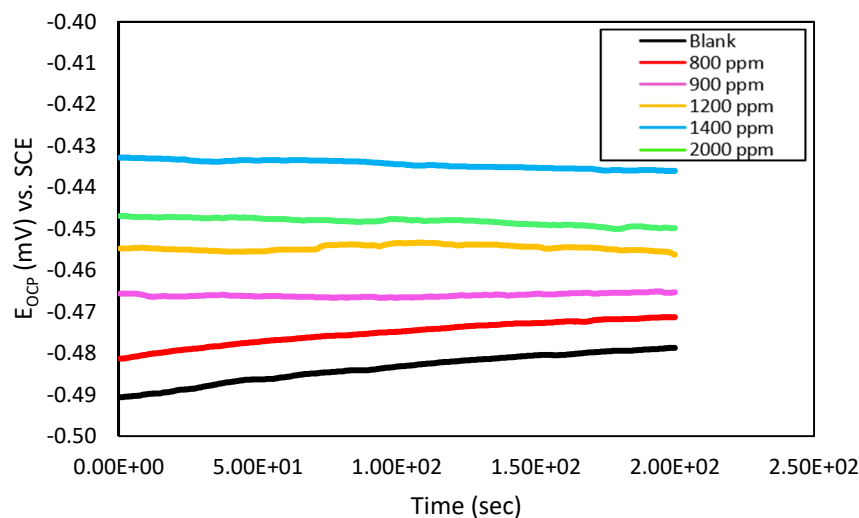


**Figure 3.** The plot of OCP for mild steel in 0.5 M HCl with and without different concentrations of DPS.

The results of open circuit potential are recorded in Table 1. It is observed that the steady-state values of OCP are more negative in uninhibited solution, and the addition of DPS inhibitor concentrations shifts the OCP of the mild steel to more negative values. This negative shift of the OCP can be attributed to forming of a protective film of the DPS inhibitor on the mild steel surface.

**Table 1.** Open circuit potential results of the electrochemical test with and without different concentrations of DPS.

| Concentrations | $E_{OCP}$ mV |
|---|---|
| Blank | −478.7 |
| 800 mg/L | −471.3 |
| 900 mg/L | −465.1 |
| 1200 mg/L | −446.9 |
| 1400 mg/L | −432.8 |
| 2000 mg/L | −439.2 |

*3.2. Potentiodynamic Polarisation*

Polarisation measurements are suitable for monitoring the mechanisms and progress of the anodic and cathodic reactions. Potentiodynamic polarisation tests were conducted to determine the effects of the cathodic ($2H^+ + 2e \rightarrow H_2$) and anodic ($Fe \rightarrow Fe^{2+} + 2e$) reactions of the corrosion process. Furthermore, potentiodynamic polarisation curves for mild steel in 0.5 M HCl with and without the presence of DPS are shown in Figure 4. The plots displayed the reactions of cathodic and anodic in a blank solution and the adjunct DPS, which was based on the law of Tafel. Densities of corrosion were determined from the linear Tafel sections of the cathodic and anodic curves. Table 2 displays the parameters ($i_{corr}$) as the corrosion current densities, ($E_{corr}$) as the potential for corrosion, and the Tafel slope for anodic ($\beta_a$) and for cathodic ($\beta_c$), which was obtained from the curve polarisation. It is indicated from the results in Table 2 that the $i_{corr}$ decreased in the presence of DPS compared to the blank solution. Furthermore, it was also determined that no significant shift was made by the inhibitor on the ($E_{corr}$). A compound is usually categorised as a cathodic or an anodic type inhibitor when the shift in ($E_{corr}$) is more significant than 85 mV [28,29].
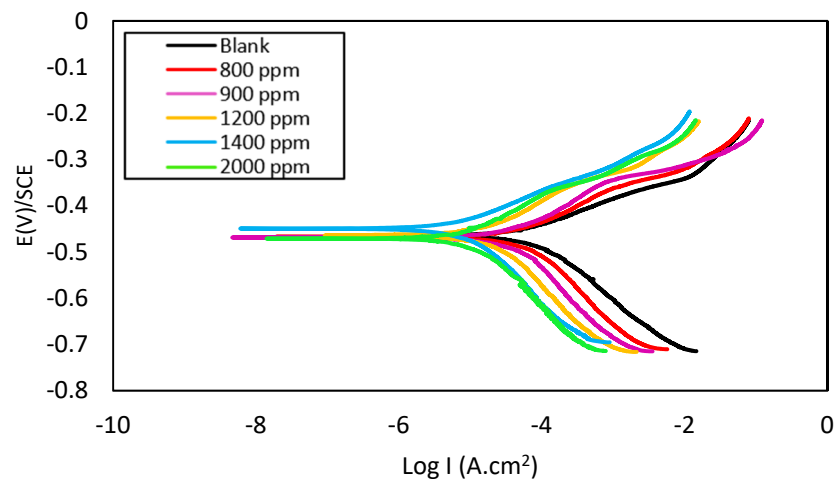


**Figure 4.** Potentiodynamic polarisation curves in 0.5 M HCl for mild steel with various concentration levels of DPS.

**Table 2.** Potentiodynamic polarisation characteristics in 0.5 M HCl with and without DPS for mild steel.

| Concentrations | $i_{corr}$ (μA.cm$^{-2}$) | $E_{corr}$ (mV) | $B_a$ (mV/dec) | $B_c$ (mV/dec) | IE% |
|---|---|---|---|---|---|
| Blank | 124 | −455 | 79.9 | −126.7 | 0 |
| 800 mg/L | 39 | −465 | 69.1 | −148.6 | 69 |
| 900 mg/L | 32 | −470 | 60.4 | −119.8 | 75 |
| 1200 mg/L | 18 | −469 | 64.9 | −123.7 | 86 |
| 1400 mg/L | 6 | −467 | 68.8 | −143.7 | 95 |
| 2000 mg/L | 10 | −471 | 61.3 | −104.9 | 92 |

As a result, the largest shift of ($E_{corr}$) amounted to 7 mV, indicating the classification of the inhibitor as a mixed type. A similar result was obtained in other studies of green corrosion inhibitors in an acidic medium [30]. Specifically, although the inhibitor did not influence the cathodic hydrogen evolution mechanism, it decreased the $H^+$ ions on the mild steel surface through a charge transfer mechanism. The absorption of the atoms of the inhibitor occurred by hindering the locales of responses on the mild steel surface. Although this phenomenon decreased the existing surface area for hydrogen evolution, the mechanism reaction for hydrogen was not affected [31].

Table 2 illustrates that the increase in IE from 69% to 95% took place, including the attraction of the total DPS particles towards the surface of mild steel and a hindrance to the dissolution process. Furthermore, the IE% decreased to 92% at 2000 mg/L. The $i_{corr}$ decreased in the inhibitor solution compared with the 0.5 M HCl (blank solution). The potential gap ($E_{corr}$) between the medium in the absence and presence of the inhibitor was 12 mV, which is less than 85 mV. In addition, such minor discrepancies in the values of $E_{corr}$ demonstrate the "stability" of the steel surface that is exposed to the aggressive behaviour of chlorides [32].

This indicated that the DPS is a mixed-type inhibitor for mild steel in 0.5 M HCl. This means that the inhibitor influenced both anodic and cathodic corrosion processes on the mild steel surface.

### 3.3. Electrochemical Impedance Spectroscopy (EIS)

To classify the kinetic characteristics and the electrochemical procedures of mild steel in 0.5 M HCl, including the ways in which DPS modified them, EIS studies were conducted. Figure 5a illustrates the Nyquist plot, and Figure 5b illustrates Bode plots with and without the various concentrations of DPS for mild steel corrosion in 0.5 M HCl. The Nyquist plots are made up of single depressed capacitive loops, indicating that the corrosion of mild steel in the HCl medium is governed by a charge transfer process [33]. The interception of the low frequency with the real axis was ascribed to the charge transfer resistance ($R_{ct}$), and the high frequency in the real axis in the Nyquist plot was earmarked for the solution resistance ($R_s$). Furthermore, the absorption of DPS particles on the surface of mild steel with different inhibition efficiency and the natural ability of DPS represented the simplification of the inhibitor's impacts corresponding to the blank solutions, indicating the corrosion procedure's inhibition.

The electrochemical parameters acquired from the Nyquist plot for mild steel corrosion in 0.5 M HCl with and without various concentrations of DPS are recorded in Table 3. It was determined that the DPS increased the values of $R_{ct}$, which were related to the expansion in the diameter of the Nyquist semicircle. The maximum 1E% was achieved at the optimum concentration of 1400 mg/L because this is the critical concentration. The efficiency of the corrosion inhibitor is at its optimum level when the inhibitor concentrations reach critical micellisation concentration (CMC). When the concentration is less than the CMC level, the steel surface is increasingly covered by adsorbed inhibitors at the sub-monolayer to monolayer.

The IE% rises rapidly as the inhibitor molecules occupy more active sites. At the same time, the efficiency decreases at 2000 mg/L of inhibitor concentration. This condition is caused by the micellisation of inhibitor molecules, which occurs when a CMC is exceeded. Once the CMC is reached, the steel surface is thought to be wholly covered by a monolayer, sufficient for effective inhibition. Further concentration growth results in forming a multi-layered configuration. These extra layers of inhibitor molecules do not contribute much to the protection supplied by the monolayer. They only add to the resistance to oxidant supply and reaction product transport, resulting in minor differences in inhibition efficiency.
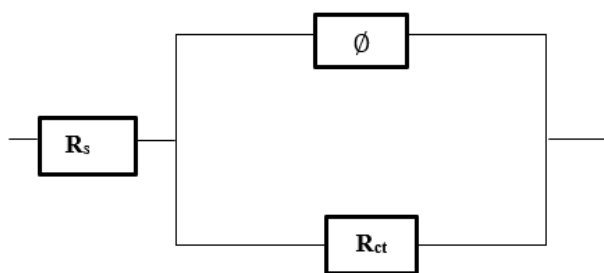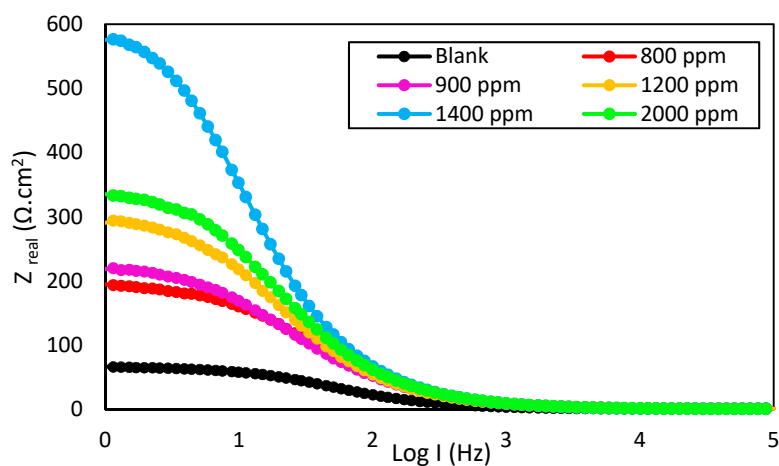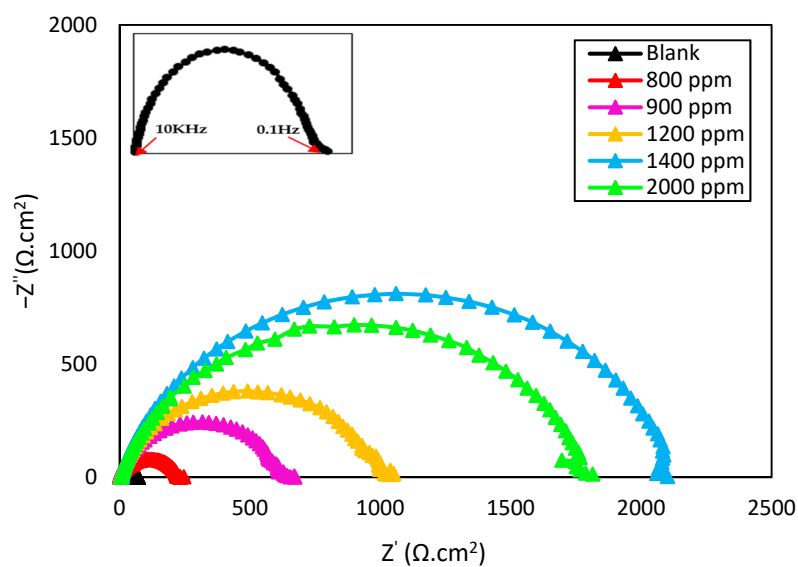
**Figure 5.** Electrochemical impedance for mild steel (**a**) Nyquist plot, (**b**) Bode plot in 0.5 M HCl with and without different concentrations of DPS and (**c**) the equivalent circuit used to match the Nyquist data.

**Table 3.** The EIS parameters for mild steel in 0.5 M HCl, with and without DPS.

| Concentrations | $R_{ct}$ ($\Omega cm^2$) | $R_s$ ($\Omega cm^2$) | IE% |
|---|---|---|---|
| blank | 40.43 | 622 | 0 |
| 800 mg/L | 120 | 197 | 66 |
| 900 mg/L | 190 | 228 | 79 |
| 1200 mg/L | 300 | 626 | 87 |
| 1400 mg/L | 900 | 790 | 96 |
| 2000 mg/L | 701 | 821 | 94 |

In the presence of an inhibitor, the increase in $R_{ct}$ led to higher IE%. This pattern indicated an excellent protective layer formed on the surface of mild steel, suggesting that all DPS particles were absorbed into the surface.

*3.4. Weight Loss Test*

The weight loss test was performed at 25 °C after 24 h of immersion in 0.5 M HCl solution in the presence and absence of different concentrations of DPS. The results of steel weight loss in 0.5 M HCl are summarised in Table 4. It has been observed from the results that the corrosion rates decreased; meanwhile, the IE% and adsorption coverage of the inhibitor on the mild steel surface increased as the inhibitor concentration increased. The maximum IE was 91% at the optimum concentration of 1400 mg/L. The IE was observed to decrease when the 2000 mg/L of inhibitor was applied; this observation could be ascribed to the saturation of inhibitor composites within the corrosive fluid, restricting composite inhibitor interaction with the metal surface and reducing IE%.

**Table 4.** Weight loss occurs after 24 h of immersion with different concentrations of DPS.

| Concentrations | $C_r$ (mmy$^{-1}$) | IE% | θ |
|---|---|---|---|
| Blank | 2.508 | - | - |
| 800 mg/L | 0.895 | 64 | 0.64 |
| 900 mg/L | 0.672 | 73 | 0.73 |
| 1200 mg/L | 0.396 | 84 | 0.84 |
| 1400 mg/L | 0.228 | 91 | 0.91 |
| 2000 mg/L | 0.292 | 88 | 0.88 |

*3.5. Scanning Electron Microscopy*

The scanning electron microscopy (SEM) analysis was performed under 3000× magnification to study the mild steel surface. This examination was carried out at room temperature after 24 h of immersion time for three samples. From the micrographs, the following points are derived: (1) The SEM image on the polished mild steel surface before being exposed to the corrosive solution shows a smooth surface with no visible marks, as shown in Figure 6a. (2) It can be seen that the surface of mild steel immersed in 0.5 M has several corrosion holes that developed on the metal surface and that were found severely deteriorated, as described in Figure 6b. (3) When the immersion test was repeated in the presence of 1400 mg/L of DPS corrosion inhibitor, significant corrosion suppression was noted with a relatively smooth surface. Therefore, the mild steel surface is protected by the adsorbed DPS inhibitor, as exhibited in Figure 6c.
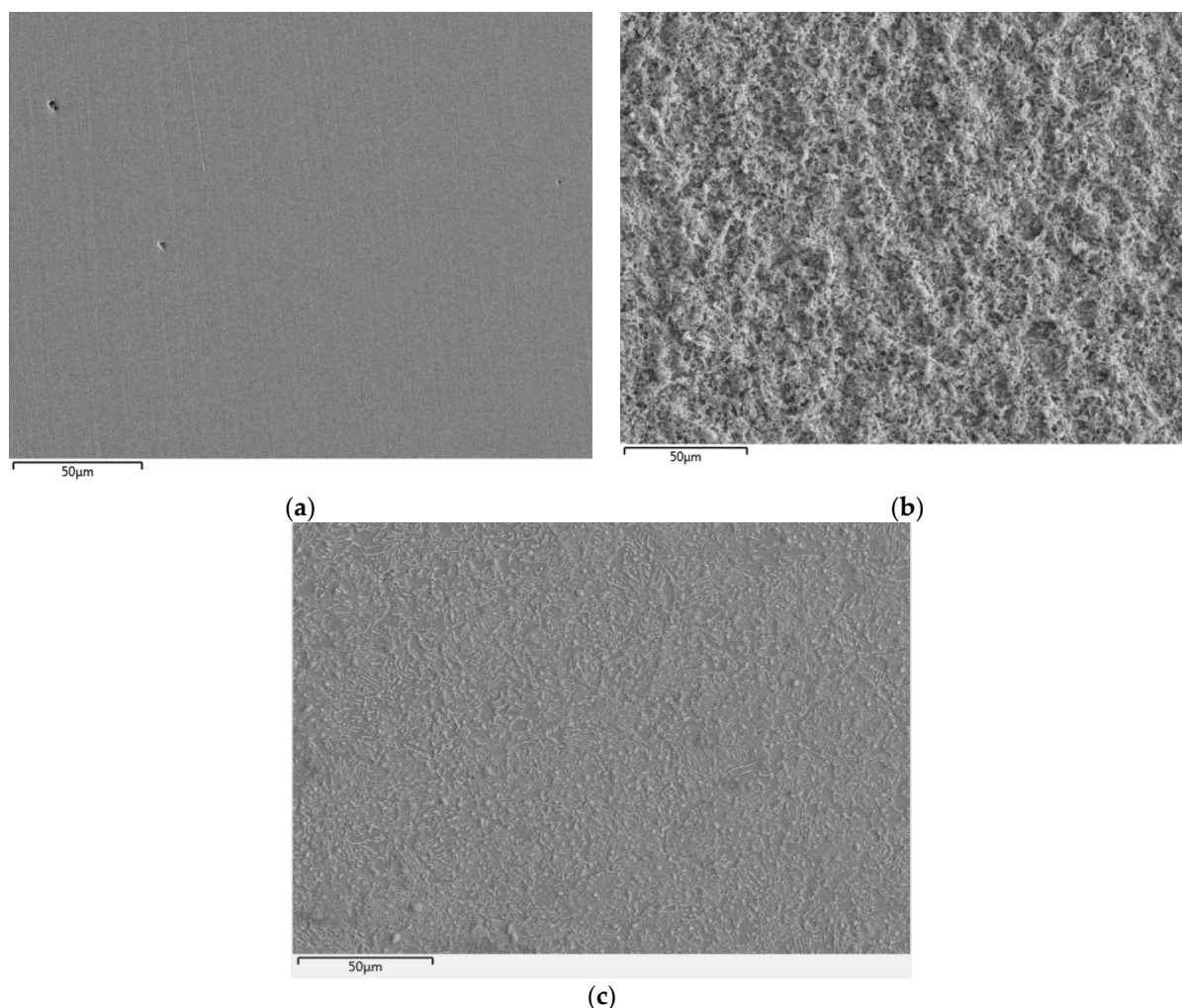
(a)

(b)



(c)

**Figure 6.** SEM micrographs of mild steel in 0.5 M HCl: (**a**) polished sample, (**b**) without DPS, and (**c**) with 1400 mg/L of DPS.

### 3.6. Fourier Transform Infrared Spectroscopy (FTIR) Analysis

Figure 7 shows the FTIR spectrum of the fatty acid in DPS, and its respective FTIR peaks are shown in Table 5. The peaks at 584 cm$^{-1}$ to 721 cm$^{-1}$ represent C=C stretching. The peaks describe the stretching vibration of the C-O ester groups and the CH$_2$ wag in the 852 and 1114 cm$^{-1}$ areas. The peaks at 963.37 cm$^{-1}$ show the O$-$H bend, while C-O stretching alcohol groups are represented in the 1157 cm$^{-1}$ peak. The bending vibrations of CH$_2$ and CH$_3$ aliphatic groups, such as symmetric H-C-H bending at 1376 cm$^{-1}$ and CH$_2$ scissoring at 1457–1585 cm$^{-1}$, are generally ascribed to the peaks in the 1232–1418 cm$^{-1}$ region. The C=C stretching vibration of carboxylic acids in the ester is responsible for the peak at 1743 cm$^{-1}$. The stretching vibrations of aliphatic C-H in CH$_2$ and terminal CH$_3$ groups are ascribed to the peaks centred at 2921 cm$^{-1}$ and 2852 cm$^{-1}$, respectively. The bending and stretching vibrations of the O-H bonds of the H$_2$O molecule in the extract correspond to the two tiny peaks at 1652 cm$^{-1}$ [34].
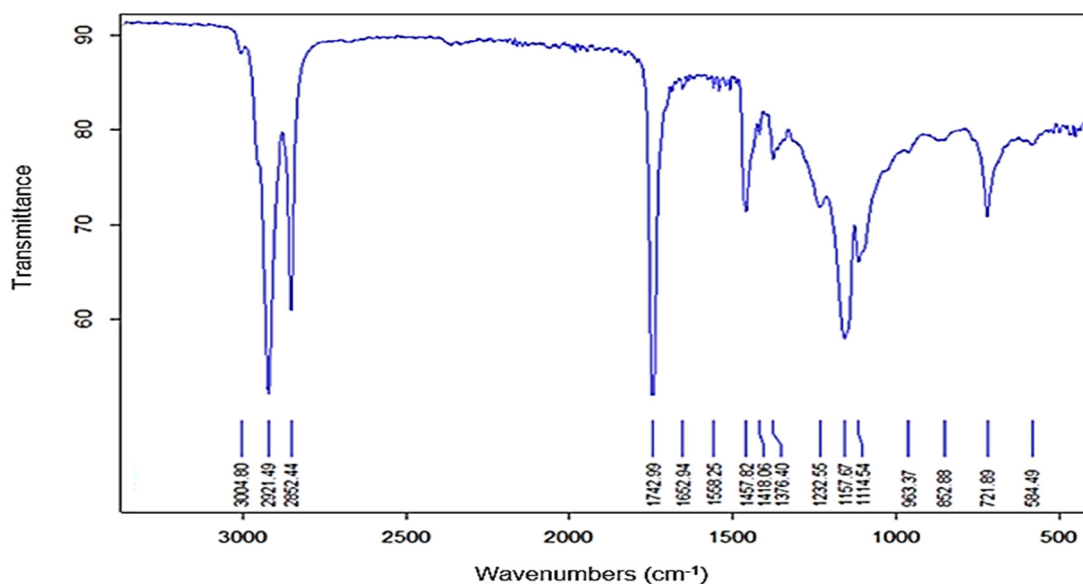
**Figure 7.** Fourier transform infrared spectroscopy of DPS.

**Table 5.** Determinant peaks for DPS via FTIR.

| The Wavenumber (cm$^{-1}$) of the Main Peaks Detected in This Study | Possible Functional Groups in Fatty Acid |
|:---:|:---:|
| 584 | C=C |
| 721 | C=C |
| 963.37 | O$-$H bend |
| 852 and 1114 | C-O and CH$_2$ |
| 1157 | C-O |
| 1376 | H-C-H bending, CH$_2$ and CH$_3$ |
| 1457 and 1585 | H-C-H bending and CH$_2$ |
| 1232 and 1418 | CH$_2$ |
| 1743 | C=C |
| 2921 and 2852 | C-H in CH$_2$ and terminal CH$_3$ groups |
| 1652 cm$^{-1}$ | O-H bonds of the H$_2$O molecule |

### 3.7. Computational of Density Function Theory (DFT)

3.7.1. Quantum Chemical Calculations

To understand the mechanism of inhibition offered by lauric, myristic, oleic, phthalic, caprylic, and palmitic acids on the Fe surface, the parameters of quantum chemicals listed in Table 6 were calculated [35]. An inhibitor's $E_{HOMO}$, $E_{LUMO}$, and $\Delta E$ values can be used to predict its performance. $E_{HOMO}$ explains the inhibitor molecule's ability to contribute electrons to the metal surface. In contrast, $E_{LUMO}$ describes the inhibitor molecule's ability to obtain electrons from the metal surface. Higher $E_{HOMO}$ values indicate a greater proclivity to donate electrons to the metal surface of the unoccupied d-orbital. Increasing $E_{HOMO}$ values facilitate adsorption on the metal surface, improving inhibition effectiveness.

**Table 6.** The specifications of fatty acids in DPS can be obtained by employing DFT.

| Fatty Acids | $E_{HOMO}$ | $E_{LUMO}$ | $\Delta E$ | IP | EA | $\chi$ | $\eta$ | $\sigma$ | $\Delta N$ |
|---|---|---|---|---|---|---|---|---|---|
| Lauric | −6.255 | −0.979 | 5.276 | 6.255 | 0.979 | 3.617 | 2.638 | 0.3791 | 0.2280 |
| Myristic | −6.258 | −0.972 | 5.286 | 6.258 | 0.972 | 3.615 | 2.643 | 0.3784 | 0.2280 |
| Oleic | −5.539 | −0.991 | 4.548 | 5.539 | 0.991 | 3.265 | 2.274 | 0.4398 | 0.3419 |
| Phthalic | −6.404 | −2.924 | 3.480 | 6.404 | 2.924 | 4.664 | 1.740 | 0.5747 | 0.0448 |
| Caprylic | −6.244 | −1.028 | 5.216 | 6.244 | 1.028 | 3.636 | 2.608 | 0.3834 | 0.2270 |
| Palmitic | −6.260 | −0.973 | 5.287 | 6.260 | 0.973 | 3.617 | 2.644 | 0.3783 | 0.2276 |

In contrast, inhibitors with lower $E_{LUMO}$ values exhibit a high ability to accept electrons. According to Table 6, oleic acid has a high $E_{HOMO}$ value, indicating a greater tendency to provide electrons to the Fe surface. In comparison, phthalic acid's lower $E_{LUMO}$ value has a higher tendency to allow electrons, followed by the Fe surface.

Another quantum chemical parameter that can be correlated with inhibition efficiency is the energy gap ($\Delta E$), which is defined as the difference between $E_{LUMO}$ and $E_{HOMO}$.

Hard molecules with a high $\Delta E$ cannot be effective corrosion inhibitors. Nonetheless, soft molecules with low $\Delta E$ could be excellent corrosion inhibitors due to their ability to donate electrons to metals easily. The $\Delta E$ can reveal the ability to donate electrons and measure the interaction between inhibitor molecules and the Fe surface. The fatty acid with low $\Delta E$ values, as is well known, provides better inhibition performance. This is due to the low excitation energy required to remove an electron from the last occupied orbital.

Our result in Table 6 displays that phthalic acid has a low $\Delta E$ value, indicating greater reactivity and strong inhibition performance on the Fe surface. Global hardness ($\eta$) and softness ($\sigma$) are terms used to describe the resistance of atoms to the deformation of their electron cloud [36]. These are critical properties for calculating molecular stability and reactivity. Phthalic acid has the lowest $\eta$ value of 1.740 eV. Meanwhile, the oleic acid has the highest $\sigma$ value of 0.3783 eV, which is assumed to be the most effective corrosion inhibitor. The number of electrons transferred ($\Delta N$) was higher for oleic acid, indicating a stronger proclivity to contribute electrons to the Fe surface [37]. According to the findings, the values of $\Delta N$ in this study were positive, which indicates that the molecules of fatty acid act as electron donors [38].

The distribution of HOMO electron density over the inhibitor in Table 7 indicates that the inhibitor molecule is likely to be active in electron donation to the empty Fe orbital, resulting in efficient corrosion inhibition. On the other hand, the distribution of LUMO density across the molecule confirms that electrons from the occupied Fe orbitals can be effectively accepted, which is a critical factor for interactions between the donor and acceptor. The HOMO and LUMO of lauric, myristic, phthalic, caprylic, and palmitic acid molecules can be found primarily around the carboxyl (COOH) group. In the case of oleic acid, however, the HOMO was mainly localised on the C=C bond, which is consistent with another report [39]. As a result, these are the most active sites for electron donation–acceptance interactions and are most likely to facilitate adsorption over the Fe surface. Furthermore, the HOMO-LUMO distribution indicates that all double bonds in relaxed molecules serve as active HOMO sites, showing their proclivity to share electronic charges with surface metal atoms. The distribution of HOMO and LUMO around the benzene ring of phthalic acid, which has two carboxyl groups, is observed over the entire molecule.

**Table 7.** The DFT calculations for the structure and the HOMO and LUMO structures for DPS fatty acid compounds (atom legend: white = H, light grey = C, and red = O).
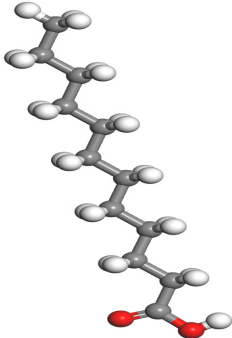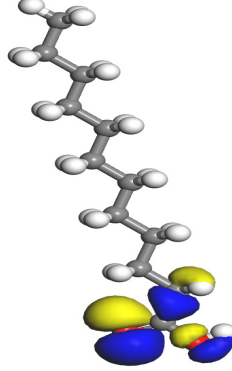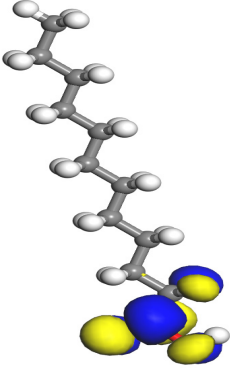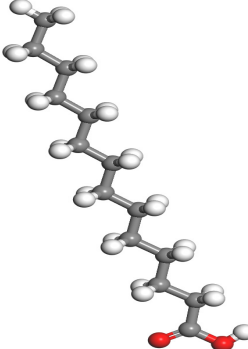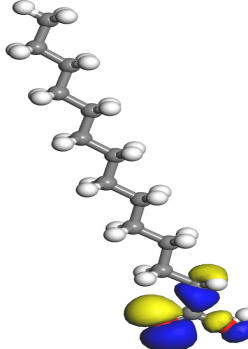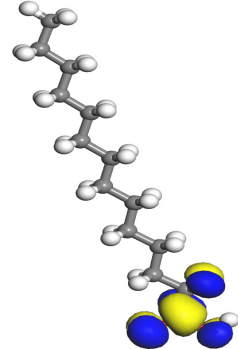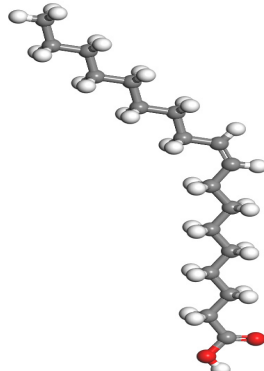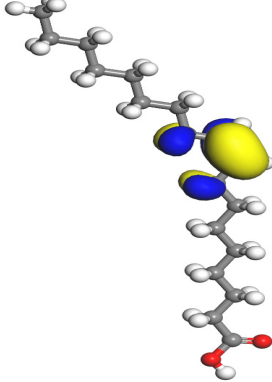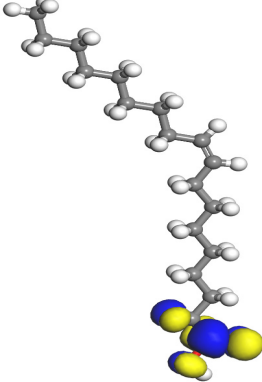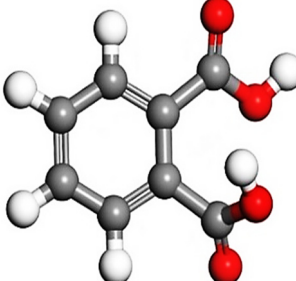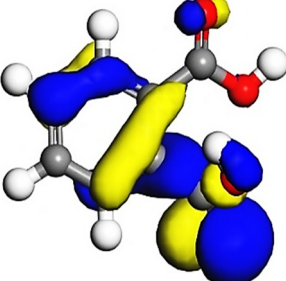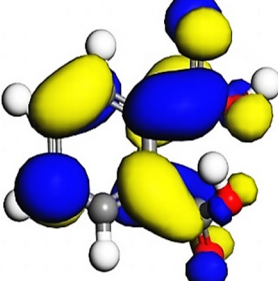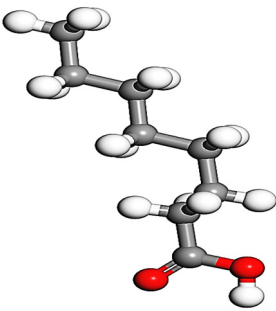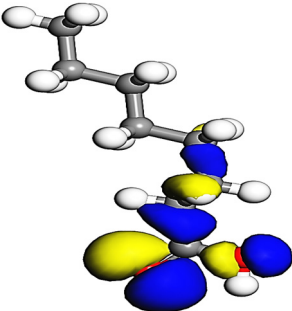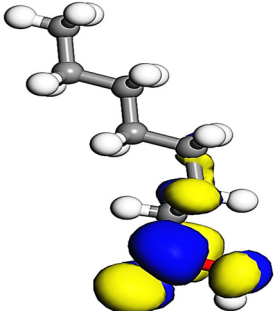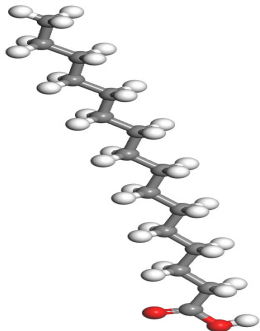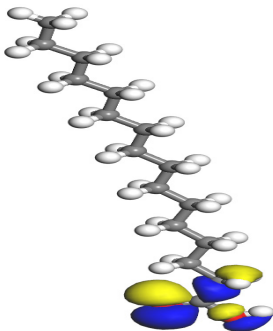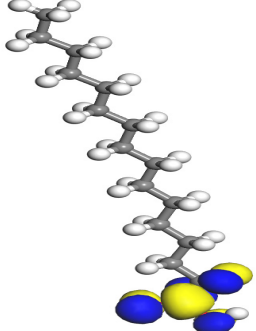
| Fatty Acids | Structure | HOMO | LUMO |
|---|---|---|---|
| Lauric | | | |
| Myristic | | | |
| Oleic | | | |
| Phthalic | | | |

**Table 7.** *Cont.*

| Fatty Acids | Structure | HOMO | LUMO |
|---|---|---|---|
| Caprylic | | | |
| Palmitic | | | |

3.7.2. Adsorption Sites

Adsorption of a corrosion inhibitor on a metal surface is enabled by electron transfer between the inhibitor molecule and the surface of metal atoms. The inhibitor can interact with a metal surface via specific atoms known as adsorption sites. To locate these sites, the Fukui functions and Mulliken atomic charge were identified. Finite functions were used to determine the local reactivity of the atoms contained in the inhibitor. The values defined by the finite functions can be used to identify the atoms in a molecule with higher reactivity to accept and lose electrons. The finite difference approximation was used to determine the electrophilic ($f^-$) and nucleophilic ($f^+$) Fukui functions as follows [40]:

$$f^- = q_k(N) - q_k(N-1), \tag{14}$$

$$f^+ = q_k(N+1) - q_k(N), \tag{15}$$

where $q_k$ is the charge of an atom, while $N-1$, $N$ and $N+1$ is the number of electrons in the cation, neutral molecule, and anion. The electrophilic ($f^-$) and nucleophilic ($f^+$) Fukui functions display the distribution density of electrons in inhibition molecules to predict the preferred sites for nucleophilic attacks and the selected sites for electrophilic attacks that are more likely to participate in the donor–acceptor type interaction with the metal surface. The high values of $f^-$ indicate that the sites belonging to a molecule are available to accept the electrons (electrophilic site) while the high values of $f^+$ show that the sites of a molecule are capable of donating electrons (nucleophilic site).

As shown in Table 8, the highest value of electrophilic ($f^-$) is assigned to O14, O16, C3, O12, O9, and O18, suggesting that these atoms form a back bond by accepting electrons from the Fe surface to the inhibitor and vice versa, while the highest value of nucleophilic ($f^+$) is assigned to C12, C14, C18, O11, C8, and C16 for lauric, myristic, oleic, phthalic, caprylic, and palmitic acid, which indicates that these atoms prefer to form a chemical bond by electrons donation to the Fe surface. In addition, the overall Fukui function data reported the significant role of double bonds and oxygen atoms in increasing the reactivity of the molecules.

**Table 8.** The Fukui indices of electrophilic ($f^-$) and nucleophilic ($f^+$) behaviours of lauric, myristic, oleic, phthalic, caprylic and palmitic acids.

| Lauric Acid | | | Myristic Acid | | | Oleic Acid | | |
|---|---|---|---|---|---|---|---|---|
| Atom | $f^-$ | $f^+$ | Atom | $f^-$ | $f^+$ | Atom | $f^-$ | $f^+$ |
| C1 | −0.003 | −0.002 | C1 | −0.002 | −0.002 | C1 | −0.043 | −0.004 |
| C2 | −0.004 | −0.003 | C2 | −0.003 | −0.002 | C2 | −0.043 | −0.002 |
| C3 | −0.004 | −0.003 | C3 | −0.003 | −0.002 | C3 | 0.152 | 0.008 |
| C4 | −0.004 | −0.003 | C4 | −0.003 | −0.002 | C4 | 0.151 | 0.010 |
| C5 | −0.005 | −0.005 | C5 | −0.003 | −0.002 | C5 | −0.025 | −0.002 |
| C6 | −0.007 | −0.006 | C6 | −0.004 | −0.003 | C6 | −0.017 | −0.001 |
| C7 | −0.009 | −0.009 | C7 | −0.005 | −0.005 | C7 | −0.011 | −0.001 |
| C8 | −0.012 | −0.013 | C8 | −0.007 | −0.006 | C8 | −0.008 | −0.001 |
| C9 | −0.020 | −0.023 | C9 | −0.010 | −0.009 | C9 | −0.006 | −0.001 |
| C10 | −0.042 | −0.031 | C10 | −0.012 | −0.012 | C10 | −0.005 | −0.001 |
| C11 | −0.013 | −0.068 | C11 | −0.020 | −0.024 | C11 | −0.004 | −0.001 |
| C12 | 0.128 | 0.273 | C12 | −0.041 | −0.028 | C12 | −0.025 | −0.007 |
| O13 | 0.090 | 0.110 | C13 | −0.013 | −0.070 | C13 | −0.017 | −0.009 |
| O14 | 0.370 | 0.231 | C14 | 0.123 | 0.273 | C14 | −0.010 | −0.013 |
| | | | O15 | 0.087 | 0.111 | C15 | −0.007 | −0.022 |
| | | | O16 | 0.356 | 0.232 | C16 | −0.006 | −0.031 |
| | | | | | | C17 | −0.004 | −0.068 |
| | | | | | | C18 | 0.002 | 0.272 |
| | | | | | | O19 | 0.004 | 0.119 |
| | | | | | | O20 | 0.005 | 0.226 |

| Phthalic acid | | | Caprylic acid | | | Palmitic acid | | |
|---|---|---|---|---|---|---|---|---|
| Atom | $f^-$ | $f^+$ | Atom | $f^-$ | $f^+$ | Atom | $f^-$ | $f^+$ |
| C1 | 0.043 | 0.034 | C1 | −0.007 | −0.007 | C1 | −0.002 | −0.001 |
| C2 | 0.018 | 0.077 | C2 | −0.009 | −0.009 | C2 | −0.003 | −0.001 |
| C3 | 0.022 | 0.014 | C3 | −0.011 | −0.011 | C3 | −0.002 | −0.001 |
| C4 | 0.005 | 0.058 | C4 | −0.016 | −0.018 | C4 | −0.002 | −0.001 |
| C5 | 0.024 | 0.047 | C5 | −0.017 | −0.017 | C5 | −0.003 | −0.002 |
| C6 | 0.026 | 0.032 | C6 | −0.021 | −0.038 | C6 | −0.003 | −0.002 |
| C7 | 0.017 | 0.089 | C7 | −0.025 | −0.052 | C7 | −0.003 | −0.003 |
| O8 | 0.001 | 0.047 | C8 | 0.115 | 0.277 | C8 | −0.004 | −0.003 |
| O9 | 0.068 | 0.043 | O9 | 0.375 | 0.226 | C9 | −0.005 | −0.005 |
| C10 | 0.092 | 0.025 | O10 | 0.119 | 0.117 | C10 | −0.007 | −0.006 |
| O11 | 0.084 | 0.114 | | | | C11 | −0.009 | −0.009 |
| O12 | 0.289 | 0.076 | | | | C12 | −0.012 | −0.013 |
| | | | | | | C13 | −0.018 | −0.023 |
| | | | | | | C14 | −0.040 | −0.029 |
| | | | | | | C15 | −0.011 | −0.069 |
| | | | | | | C16 | 0.117 | 0.273 |
| | | | | | | O17 | 0.082 | 0.111 |
| | | | | | | O18 | 0.338 | 0.232 |

Mulliken charges were used to calculate the charge across the entire skeleton of the molecule. The Mulliken charges calculated for lauric, myristic, oleic, phthalic, caprylic and palmitic acids are presented in Table 9. For the Mulliken charge distribution, C12, C14, C18, C10, C8 and C16 appear to be of the highest positive charge. In contrast, O13, O15, O19 O8, O10 and O17 appear to be of the highest negative charge for atoms in lauric, myristic, oleic, phthalic, caprylic and palmitic acids. It is well known that the more negative the calculated charge, the more efficiently the atom donates its electron to the unoccupied orbital of the Fe surface; thus, its inhibition efficiency increases. The O and C atoms with negative charge sites could offer electrons to the Fe surface to form a coordinate bond.

**Table 9.** The Mulliken charge distribution of lauric, myristic, oleic, phthalic, caprylic and palmitic acids.

| Lauric Acid | | Myristic Acid | | Oleic Acid | |
|---|---|---|---|---|---|
| **Atom** | **Mulliken Charge** | **Atom** | **Mulliken Charge** | **Atom** | **Mulliken Charge** |
| C1 | −0.247 | C1 | −0.245 | C1 | −0.195 |
| C2 | −0.151 | C2 | −0.153 | C2 | −0.195 |
| C3 | −0.146 | C3 | −0.146 | C3 | −0.042 |
| C4 | −0.147 | C4 | −0.147 | C4 | −0.041 |
| C5 | −0.148 | C5 | −0.149 | C5 | −0.158 |
| C6 | −0.149 | C6 | −0.149 | C6 | −0.153 |
| C7 | −0.150 | C7 | −0.150 | C7 | −0.149 |
| C8 | −0.150 | C8 | −0.150 | C8 | −0.148 |
| C9 | −0.151 | C9 | −0.150 | C9 | −0.146 |
| C10 | −0.146 | C10 | −0.151 | C10 | −0.152 |
| C11 | −0.279 | C11 | −0.152 | C11 | −0.246 |
| C12 | 0.525 | C12 | −0.143 | C12 | −0.158 |
| O13 | −0.418 | C13 | −0.283 | C13 | −0.154 |
| O14 | −0.378 | C14 | 0.527 | C14 | −0.151 |
| | | O15 | −0.419 | C15 | −0.150 |
| | | O16 | −0.378 | C16 | −0.144 |
| | | | | C17 | −0.246 |
| | | | | C18 | 0.520 |
| | | | | O19 | −0.429 |
| | | | | O20 | −0.406 |

| Phthalic acid | | Caprylic acid | | Palmitic acid | |
|---|---|---|---|---|---|
| **Atom** | **Mulliken charge** | **Atom** | **Mulliken charge** | **Atom** | **Mulliken charge** |
| C1 | −0.063 | C1 | −0.247 | C1 | −0.245 |
| C2 | −0.057 | C2 | −0.153 | C2 | −0.153 |
| C3 | −0.067 | C3 | −0.144 | C3 | −0.146 |
| C4 | −0.003 | C4 | −0.156 | C4 | −0.147 |
| C5 | 0.009 | C5 | −0.154 | C5 | −0.149 |
| C6 | −0.064 | C6 | −0.174 | C6 | −0.150 |
| C7 | 0.447 | C7 | −0.228 | C7 | −0.150 |
| C8 | −0.412 | C8 | 0.513 | C8 | −0.151 |
| C9 | −0.409 | O9 | −0.406 | C9 | −0.151 |
| C10 | 0.475 | O10 | −0.425 | C10 | −0.151 |
| O11 | −0.406 | | | C11 | −0.151 |
| O12 | −0.372 | | | C12 | −0.151 |
| | | | | C13 | −0.152 |
| | | | | C14 | −0.146 |
| | | | | C15 | −0.282 |
| | | | | C16 | 0.525 |
| | | | | O17 | −0.418 |
| | | | | O18 | −0.377 |

*3.8. Comparison with Related Work*

Scientific researchers used plant parts such as leaves, seeds, fruit, and roots as corrosion inhibitors. Table 10 summarises the plant source, source of bio-waste, major constituent responsible for inhibition, max IE%, and theoretical calculations. Most studies focused on the corrosion inhibition of carbon steel and mild steel due to their widespread use in the industry compared to other ferrous metals and their poor acid corrosion resistance. Most of the literature on acidic media investigated corrosion inhibition in acid solutions. Organic compounds from various parts of palm tree sources as corrosion inhibitors have been widely reported. However, the studies that have been conducted by the previous literature are still limited to specific parameters and the scope of the study. From Table 10, it is clear that we used a DFT simulation in this study compared to others (from #1 to #7)

where it was not incorporated, which provided an advantage to our inhibitor. In addition, the efficiency of the proposed inhibitor is higher than that of the others (from #1 to #7).

**Table 10.** Comparison with different plants as a green corrosion inhibitor.

| # | Plant or Source of GCI | Is It a Source of Bio-Waste? | Major Constituent | Metal | Electrolyte | Max IE% | C | Applied DFT | Ref |
|---|---|---|---|---|---|---|---|---|---|
| 1 | Date palm seed | Yes | Fatty acid | Carbon steel | 0.5 $H_2SO_4$ | 88 | 2000 mg/L | No | [41] |
| 2 | *Dysphania ambrosioides* | No | Fatty acid | Mild steel | 1 M HCl | 84 | 1.5 g/L | No | [42] |
| 3 | *Terminalia arjuna* leaves | Yes | - | Mild steel | 0.2 M HCl | 64 | - | No | [43] |
| 4 | *Chamaerops humilis* L. fruit | No | - | Mild steel | 1 M HCl | 80 | 1 g/L | No | [44] |
| 5 | Ziziphora leaves from jungles | No | Acacetin, chrysin, and thymonin compounds | Mild steel | 1 M HCl | 91 | 800 mg/L | No | [45] |
| 6 | *Pinus resinosa* | No | - | Steel Rebar | Chloride ions | 81 | 1000 mg/L | No | [46] |
| 7 | *Aerva lanata* flowers | No | Alkaloids, saponins, favonoids, and phenols | Carbon steel | 1 M HCl | 87 | 600 ppm | No | [47] |
| | Date palm seed | Yes | Fatty acid | Mild steel | 0.5 M HCl | 96 | 1400 mg/L | Yes | This work |

## 4. Conclusions

The DPS was exhibited to provide better corrosion inhibition efficiency of mild steel. The efficiency increased with inhibitor concentration and reached critical micelle concentration at 1400 mg/L of more than 96% in a 0.5 M HCl medium. The decrease and increase in βc after the addition of the inhibitor indicated that the particles of DPS can reduce the dissolution of the anode and eliminate the hydrogen evolution reaction on the cathodic surface. The results of the electrochemical study and the weight loss test are in good agreement, with the maximum IE% achieved at 1400 mg/L. Meanwhile, at 2000 mg/L, the saturation of inhibitor composites in the HCl medium led to limiting composite inhibitor interaction with the mild steel surface. SEM analysis reveals that the addition of 1400 mg/L DPS inhibitors reduced the corrosion of mild steel in 0.5 M HCl. The HOMO and LUMO of lauric, myristic, phthalic, caprylic, and palmitic acid molecules were discovered to be primarily localised around the carboxyl (COOH) groups using DFT. In the case of oleic acid, however, the HOMO is primarily localised on the C=C bond. The highest electrophilic ($f^+$) values are attributed to O14, O16, C3, O12, O9, and O18 from the adsorption sites, indicating that these atoms are in charge of building a backlink by accepting electrons from the inhibitor to the Fe surface and vice versa. In contrast, the most nucleophilic ($f^-$) values are attributed to the atoms C12, C14, C18, O11, C8, and C16 for lauric, myristic, oleic, phthalic, caprylic, and palmitic acids, which shows that these atoms prefer to form a chemical connection by electron donation to the Fe surface.

## References

1.  Lahhit, N.; Bouyanzer, A.; Desjobert, J.-M.; Hammouti, B.; Salghi, R.; Costa, J.; Jama, C.; Bentiss, F.; Majidi, L. Fennel (*Foeniculum vulgare*) essential oil as green corrosion inhibitor of carbon steel in hydrochloric acid solution. *Port. Electrochim. Acta* **2011**, *29*, 127–138. [CrossRef]
2.  Bharatiya, U.; Gal, P.; Agrawal, A.; Shah, M.; Sircar, A. Effect of corrosion on crude oil and natural gas pipeline with emphasis on prevention by ecofriendly corrosion inhibitors: A comprehensive review. *J. Bio- Tribo-Corros.* **2019**, *5*, 35. [CrossRef]
3.  Mobin, M.; Rizvi, M. Polysaccharide from Plantago as a Green Corrosion Inhibitor for Carbon Steel in 1M HCl Solution. *Carbohydr. Polym.* **2016**, *160*, 172–183. [CrossRef]
4.  Verma, C.; Ebenso, E.E.; Bahadur, I.; Quraishi, M.A. An overview on plant extracts as environmental sustainable and green corrosion inhibitors for metals and alloys in aggressive corrosive media. *J. Mol. Liq.* **2018**, *266*, 577–590. [CrossRef]
5.  Fouda, A.S.; Etaiw, S.H.; Elnggar, W. Punica Plant extract as Green Corrosion inhibitor for C-steel in Hydrochloric Acid Solutions. *Int. J. Electrochem. Sci.* **2014**, *9*, 4866–4883.
6.  Victoria, S.N.; Prasad, R.; Manivannan, R. Psidium Guajava Leaf Extract as Green Corrosion Inhibitor for Mild steel in Phosphoric Acid. *Int. J. Electrochem. Sci.* **2015**, *10*, 2220–2238.
7.  Alaneme, K.K.; Daramola, Y.S.; Olusegun, S.J.; Afolabi, A.S. Corrosion Inhibition and Adsorption Characteristics of Rice Husk Extracts on Mild Steel Immersed in 1M $H_2SO_4$ and HCl Solutions. *Int. J. Electrochem. Sci.* **2015**, *10*, 3553–3567.
8.  Deng, S.; Li, X. Inhibition by Ginkgo leaves extract of the corrosion of steel in HCl and $H_2SO_4$ solutions. *Corros. Sci.* **2012**, *55*, 407–415. [CrossRef]
9.  Oguzie, E.E.; Oguzie, K.L.; Akalezi, C.O.; Udeze, I.O.; Ogbulie, J.N.; Njoku, V.O. Natural Products for Materials Protection: Corrosion and Microbial Growth Inhibition Using Capsicum frutescens Biomass Extracts. *ACS Sustain. Chem. Eng.* **2013**, *1*, 214–225. [CrossRef]
10. Noor, E.A. The impact of some factors on the inhibitory action of Radish seeds aqueous extract for mild steel corrosion in 1 M $H_2SO_4$ solution The impact of some factors on the inhibitory action of Radish seeds aqueous extract for mild steel corrosion in 1 M $H_2SO$. *Mater. Chem. Phys.* **2018**, *131*, 160–169. [CrossRef]
11. Zhang, M.; Guo, L.; Zhu, M.; Wang, K.; Zhang, R.; He, Z.; Lin, Y.; Leng, S.; Anadebe, V.C.; Zheng, X. Akebia trifoliate koiaz peels extract as environmentally benign corrosion inhibitor for mild steel in HCl solutions: Integrated experimental and theoretical investigations. *J. Ind. Eng. Chem.* **2021**, *101*, 227–236. [CrossRef]
12. Quraishi, M.A.; Singh, A.; Kumar, V.; Kumar, D.; Kumar, A. Green approach to corrosion inhibition of mild steel in hydrochloric acid and sulphuric acid solutions by the extract of *Murraya koenigii* leaves. *Mater. Chem. Phys.* **2010**, *122*, 114–122. [CrossRef]
13. Bammou, L.; Belkhaouda, M.; Salghi, R.; Benali, O.; Zarrouk, A.; Zarrok, H. Journal of the Association of Arab Universities for Basic Corrosion inhibition of steel in sulfuric acidic solution by the Chenopodium Ambrosioides Extracts Corrosion inhibition of steel in sulfuric acidic solution by the Chenopodium Ambrosioides Extracts. *J. Assoc. Arab. Univ. Basic Appl. Sci.* **2018**, *16*, 83–90. [CrossRef]
14. Saxena, A.; Prasad, D.; Haldhar, R. Use of Butea monosperma Extract as Green Corrosion Inhibitor. *Int. J. Electrochem. Sci.* **2017**, *12*, 8793–8805. [CrossRef]
15. Shahrabi Farahania, B.; Ramezanzadeh, M.J. Electrochemical and surface characterisations of morus alba pendula leaves extract (MAPLE) as a green corrosion inhibitor for steel in 1 M HCl. *J. Taiwan Inst. Chem. Eng.* **2016**, *63*, 436.
16. Alvarez, P.E.; Fiori-bimbi, M.V.; Neske, A.; Brandán, S.A.; Gervasi, C.A. Rollinia occidentalis extract as green corrosion inhibitor for carbon steel in HCl solution. *J. Ind. Eng. Chem.* **2017**, *58*, 92. [CrossRef]
17. Buchweishaija, J. Phytochemicals as green corrosion inhibitors in various corrosive media: A review. *Tanzan. J. Sci.* **2009**, *35*, 77–92.
18. Umoren, S.A.; Gasem, Z.M.; Obot, I.B. Date palm (*Phoenix dactylifera*) leaf extract as an eco-friendly corrosion inhibitor for carbon steel in 1M hydrochloric acid solution. *Anti-Corros. Methods Mater.* **2015**, *1*, 19. [CrossRef]
19. Al-senani, G.M.; Alshabanat, M. Study the Corrosion Inhibition of Carbon Steel in 1 M HCl Using Extracts of Date Palm Waste. *Int. J. Electrochem. Sci.* **2018**, *13*, 3777–3788. [CrossRef] [PubMed]
20. Mohammed, N.J.; Othman, N.K.; Taib, M.F.M.; Samat, M.H.; Yahya, S. Experimental and Theoretical Studies on Extract of Date Palm Seed as a Green Anti-Corrosion Agent in Hydrochloric Acid Solution. *Molecules* **2021**, *26*, 3535. [CrossRef]
21. Jasim, N.; Othman, N.K. Date Palm Seed Extract as a Green Corrosion Inhibitor in 0.5 M HCl Medium for Carbon Steel: Electrochemical Measurement and Weight Loss Studies. *Int. J. Electrochem. Sci.* **2020**, *15*, 9597–9610. [CrossRef]
22. Musa, A.Y.; Kadhum, A.A.H.; Mohamad, A.B.; Takriff, M.S.; Chee, E.P. Inhibition of aluminum corrosion by phthalazinone and synergistic effect of halide ion in 1.0 M HCl. *CAP* **2012**, *12*, 325–330. [CrossRef]
23. Lowmunkhong, P.; Ungthararak, D.; Sutthivaiyakit, P. Tryptamine as a corrosion inhibitor of mild steel in hydrochloric acid solution. *Corros. Sci.* **2010**, *52*, 30–36. [CrossRef]
24. Shahmoradi, A.R.; Ranjbarghanei, M.; Javidparvar, A.A.; Guo, L.; Berdimurodov, E.; Ramezanzadeh, B. Theoretical and surface/electrochemical investigations of walnut fruit green husk extract as effective inhibitor for mild-steel corrosion in 1M HCl electrolyte. *J. Mol. Liq.* **2021**, *338*, 116550. [CrossRef]
25. Berdimurodov, E.; Kholikov, A.; Akbarov, K.; Obot, I.B.; Guo, L. Thioglycoluril derivative as a new and effective corrosion inhibitor for low carbon steel in a 1 M HCl medium: Experimental and theoretical investigation. *J. Mol. Struct.* **2021**, *1234*, 130165. [CrossRef]

26.　Bhardwaj, N.; Prasad, D.; Haldhar, R. Study of the Aegle marmelos as a Green Corrosion Inhibitor for Mild Steel in Acidic Medium: Experimental and Theoretical Approach. *J. Bio- Tribo-Corros.* **2018**, *4*, 61. [CrossRef]

27.　Kokalj, A. On the HSAB based estimate of charge transfer between adsorbates and metal surfaces. *Chem. Phys.* **2012**, *393*, 1–12. [CrossRef]

28.　Reza, N.A.; Akhmal, N.H.; Fadil, N.A.; Taib, M.F.M. A review on plants and biomass wastes as organic green corrosion inhibitors for mild steel in acidic environment. *Metals* **2021**, *11*, 1062. [CrossRef]

29.　Zhang, J.; Gong, X.L.; Yu, H.H.; Du, M. The inhibition mechanism of imidazoline phosphate inhibitor for Q235 steel in hydrochloric acid medium OH. *Corros. Sci.* **2011**, *53*, 3324–3330. [CrossRef]

30.　Fragoza-mar, L.; Olivares-xometl, O.; Domínguez-aguilar, M.A.; Flores, E.A. Corrosion inhibitor activity of 1,3-diketone malonates for mild steel in aqueous hydrochloric acid solution Corrosion inhibitor activity of 1,3-diketone malonates for mild steel in aqueous hydrochloric acid solution. *Corros. Sci.* **2012**, *61*, 171–184. [CrossRef]

31.　Oguzie, E.E.; Ogukwe, C.E.; Ogbulie, J.N.; Nwanebu, F.C.; Adindu, C.B.; Udeze, I.O.; Oguzie, K.L.; Eze, F.C. Broad spectrum corrosion inhibition: Corrosion and microbial (SRB) growth inhibiting effects of Piper guineense extract. *J. Mater. Sci.* **2012**, *47*, 3592–35601. [CrossRef]

32.　Medyński, D.; Chęcmanowski, J. Corrosion Resistance of L120G13 Steel Castings Zone-Reinforced with $Al_2O_3$. *Materials* **2022**, *15*, 4090. [CrossRef]

33.　Guo, L.; Tan, J.; Kaya, S.; Leng, S.; Li, Q.; Zhang, F. Multidimensional insights into the corrosion inhibition of 3,3-dithiodipropionic acid on Q235 steel in H2SO4 medium: A combined experimental and in silico investigation. *J. Colloid. Interface Sci.* **2020**, *570*, 116–124. [CrossRef]

34.　Olowokere, J.A.; Onen, A.I.; Odineze, M.C.; B'aga, I.D.; Kefas, E.G. Extraction and Characterisation of Oil from Date Palm (*Phoenix dactylifera*) Seed. *Asian J. Appl. Chem. Res.* **2019**, *3*, 1–9.

35.　Hsissou, R. Review on epoxy polymers and its composites as a potential anticorrosive coatings for carbon steel in 3.5% NaCl solution: Computational approaches. *J. Mol. Liq.* **2021**, *336*, 116307. [CrossRef]

36.　Wang, B.-L.; Zhang, Y.; Liu, X.-H.; Zhang, L.-Y.; Zhan, Y.-Z.; Zhang, X.; Wang, L.Z.; Li, Y.H.; Li, Z.M. Synthesis and biological activity of novel dimethylpyrazole and piperazine-containing (bis) 1,2,4-triazole derivatives. *Phosphorus Sulfur Silicon Relat. Elem.* **2017**, *192*, 34–41. [CrossRef]

37.　Guo, L.; Safi, Z.S.; Kaya, S.; Shi, W.; Tüzün, B.; Altunay, N.; Kaya, C. Anticorrosive effects of some thiophene derivatives against the corrosion of iron: A computational study. *Front. Chem.* **2018**, *6*, 155. [CrossRef] [PubMed]

38.　Ituen, E.B.; Essien, E.A.; Udo, U.E.; Oluwaseyi, O.R. Experimental and theoretical study of corrosion inhibition effect of Cucumeropsis mannii N. seed oil metallic soap of zinc on mild steel surface in sulphuric acid. *Adv. Appl. Sci. Res.* **2014**, *5*, 26–53.

39.　Chandra, A.; Nguyen, M. Use of Local Softness for the Interpretation of Reaction Mechanisms. *Int. J. Mol. Sci.* **2002**, *3*, 310–323. [CrossRef]

40.　Obayes, H.R.; Al-Amiery, A.A.; Alwan, G.H.; Abdullah, T.A.; Kadhum, A.A.H.; Mohamad, A.B. Sulphonamides as corrosion inhibitor: Experimental and DFT studies. *J. Mol. Struct.* **2017**, *1138*, 27–34. [CrossRef]

41.　Ahmad, M.F.; Mohammed, N.J.; Othman, N.K. Electrochemical Studies of Date Palm Seed as a Green Corrosion Inhibitor for Carbon Steel in 0.5 M HSO and CHCOOH Conditions. In *Proceedings of the 7th International Corrosion Prevention Symposium for Research Scholars*; Springer: Berlin/Heidelberg, Germany, 2023; pp. 239–246.

42.　Daoudi, W.; El Aatiaoui, A.; Falil, N.; Azzouzi, M.; Berisha, A.; Olasunkanmi, L.O.; Dagdag, O.; Ebenso, E.E.; Koudad, M.; Aouinti, A.; et al. Essential oil of Dysphania ambrosioides as a green corrosion inhibitor for mild steel in HCl solution. *J. Mol. Liq.* **2022**, *363*, 119839. [CrossRef]

43.　Hossain, N.; Chowdhury, M.A.; Rana, M.; Hassan, M.; Islam, S. Terminalia arjuna leaves extract as green corrosion inhibitor for mild steel in HCl solution. *Results Eng.* **2022**, *14*, 100438. [CrossRef]

44.　Fekkar, G.; Yousfi, F.; Elmsellem, H.; Aiboudi, M.; Ramdani, M.; Abdel-Rahman, I.; Hammouti, B.; Bouyazza, L. Eco-friendly Chamaerops humilis L. fruit extract corrosion inhibitor for mild steel in 1M HCl. *Int. J. Corros. Scale Inhib.* **2020**, *9*, 446–459.

45.　Dehghani, A.; Bahlakeh, G.; Ramezanzadeh, B.; Ramezanzadeh, M. Potential role of a novel green eco-friendly inhibitor in corrosion inhibition of mild steel in HCl solution: Detailed macro/micro-scale experimental and computational explorations. *Constr. Build. Mater.* **2020**, *245*, 118464. [CrossRef]

46.　Subbiah, K.; Lee, H.-S.; Mandal, S.; Park, T. Conifer Cone (*Pinus resinosa*) as a Green Corrosion Inhibitor for Steel Rebar in Chloride-Contaminated Synthetic Concrete Pore Solutions. *ACS Appl. Mater. Interfaces* **2021**, *13*, 43676–43695. [CrossRef]

47.　Hynes, N.R.J.; Selvaraj, R.M.; Mohamed, T.; Mukesh, A.M.; Olfa, K.; Nikolova, M.P. Aerva lanata flowers extract as green corrosion inhibitor of low-carbon steel in HCl solution: An in vitro study. *Chem. Pap.* **2021**, *75*, 1165–1174. [CrossRef]